The interdimeric interface controls function and stability of *Ureaplasma urealiticum* methionine S-adenosyltransferase

Daniel Kleiner [1], Fannia Shmulevich [1], Raz Zarivach [1,2], Anat Shahar [2], Michal Sharon [3], Gili Ben-Nissan [3] and Shimon Bershtein [1]

1 - Department of Life Sciences, *Ben-Gurion University of the Negev, POB 653, Beer-Sheva, 84105, Israel*
2 - Macromolecular Crystallography Research Center (MCRC), *The National Institute for Biotechnology in the Negev, Ben-Gurion University of the Negev, Beer-Sheva, Israel*
3 - Department of Biomolecular Sciences, *Weizmann Institute of Science, Rehovot, Israel*

Correspondence to Shimon Bershtein: *shimonb@bgu.ac.il*
https://doi.org/10.1016/j.jmb.2019.09.003
Edited by Dan Tawfik

Abstract

Methionine S-adenosyltransferases (MATs) are predominantly homotetramers, comprised of dimers of dimers. The larger, highly conserved intradimeric interface harbors two active sites, making the dimer the obligatory functional unit. However, functionality of the smaller, more diverged, and recently evolved interdimeric interface is largely unknown. Here, we show that the interdimeric interface of *Ureaplasma urealiticum* MAT has evolved to control the catalytic activity and structural integrity of the homotetramer in response to product accumulation. When all four active sites are occupied with the product, S-adenosylmethionine (SAM), binding of four additional SAM molecules to the interdimeric interface prompts a ~45° shift in the dimer orientation and a concomitant ~60% increase in the interface area. This rearrangement inhibits the enzymatic activity by locking the flexible active site loops in a closed state and renders the tetramer resistant to proteolytic degradation. Our findings suggest that the interdimeric interface of MATs is subject to rapid evolutionary changes that tailor the molecular properties of the entire homotetramer to the specific needs of the organism.

Introduction

Methionine S-adenosyltransferases (MATs) are highly conserved enzymes found in all kingdoms of life. Bacterial and eukaryotic MATs are closely related and share more than 40% of amino acid sequence [1,2]. Although archaeal MATs do not share a conserved sequence with their bacterial or eukaryotic counterparts (~20% of sequence identity), they do exhibit a close structural resemblance with them [3,4]. MATs catalyze the only known biochemical route to formation of S-adenosylmethionine (SAM) – a metabolite involved in myriads of metabolic reactions in the cell, including methylation, polyamine synthesis, and production of cofactors [5]. MATs are predominantly dihedral homotetramers, and, as such, are comprised of dimers of dimers. The MAT monomer consists of three domains, each built of βαββαβ repeats [1]. To form a dimer, two monomers are paired in an inverted configuration such that the α-helixes are surface exposed, whereas β-strands form a large flat hydrophobic interface. The interface is isologous, as the same surface patch from both subunits participates in its formation. Two deep cavities harboring active sites are located directly in this dimeric interface. Both monomers contribute to the formation of each of the active sites, making the homodimer the obligatory functional unit. Two such dimers interact via a smaller isologous interface to form a homotetramer. Although the emergence of the first dimeric interface is clearly adaptive, determining whether the assembly of two dimers into a tetramer is a functionally beneficial result of selection is not straightforward, particularly in the light of the fact that dimeric MATs have also been reported [6,7].

What are the mechanisms governing the emergence and assembly of dihedral homotetramers? An idea has been put forward suggesting that the evolutionary route toward assembly of dihedral homotetramers can be predicted based solely on

the differences in the interface sizes [8]. According to this idea, which is based on energetic considerations, the largest interface in the dihedral homotetramer has arose first in evolution via homodimerization of two monomers. The assembly of two dimers into a tetramer, mediated by the smaller interface, then followed. The hierarchy in the sizes of the interfaces, therefore, is preserved in evolution to maintain the proper assembly route. This idea is supported by the analytical predictions and experimental findings that show that most (if not all) dihedral homotetramers indeed follow the monomer-dimer-tetramer (MDT) (dis)assembly path [8–10].

While the properties of the interfaces can teach us about the evolution of assembly of dihedral complexes, the functional contribution of the interfaces, and especially the recently evolved nonessential ones, is less obvious. Indeed, both adaptive and nonadaptive processes seem to contribute to the emergence of homomeric complexes [11]. Lynch [12,13] has demonstrated a strong dependence of the pathways for the emergence of protein complexes on the effective population size of major phylogenetic groups and suggested that protein multimerization can be a stochastic outcome of random genetic drift. Protein homomerization was also shown to emerge as a side effect to thermodynamic stabilization of the complexes, a process that does not necessarily lead to new or improved functionality [14–16]. Notwithstanding, probably all homomeric complexes possess the inherent potential for allosteric regulation [17–19] and functional activation [20,21], phenomena that can eventually be recruited by adaptive evolution. Indeed, a strong relationship has been observed between symmetry of the homomeric complexes and function they perform, suggesting that protein function is an important determinant of quaternary structure evolution. Dihedral homomers, in particular, were found to be significantly enriched with allosteric metabolic enzymes [22].

Here, we report a structure-function analysis of bacterial MATs, including the yet uncharacterized MAT from *Ureaplasma urealiticum* (uMAT). We show that the interdimeric interface plays a pivotal role in the regulation of enzymatic activity and structural integrity of uMAT homotetramer. Specifically, in response to an increase in SAM concentration, uMAT undergoes a dramatic structural rearrangement, whereby all active site loops attain a closed state facilitated by binding of SAM molecules to the interdimeric interface. Concomitantly, uMAT dimers rotate by ~45°, thus increasing the surface of the interdimeric interface by 60% and forming a continuous β-sheet that runs throughout the interdimeric interface and stiches both dimers together. This rearrangement inhibits the enzymatic catalysis and renders the tetramer resistant to proteolysis. We compare the geometry, composition, and types of interaction within the interfaces of bacterial MATs and suggest that, unlike the highly conserved and evolutionary ancient large interface, the smaller and much more diverged interdimeric interface is recruited by evolution to tune the molecular properties of the entire homotetrameric complex. By acting on the smaller interface, evolution can tailor degradation propensity, activity regulation, and other crucial properties of the complex to the particular needs of the organism, while preserving the original function and assembly path dictated by the larger interface.

Results

uMAT is a dihedral homotetramer

We began by solving the structure of uMAT in the absence of ligands. Two virtually identical crystal structures, formed under different conditions and occupying different space groups (P1 and $P2_1$), were solved by homologous replacements, each to 2.6 Å resolution (Fig. 1A, Fig. S1A, and Table 1). The overall structure of uMAT monomer is highly conserved. Comparison with MAT from *Escherichia coli* (eMAT) reveals that although eMAT and uMAT monomers share only 44% amino acid sequence identity, the root mean square deviation (RMSD) among α-carbons of both structures is as low as 1.35 Å (Fig. S1B). uMAT is a dihedral homotetramer comprised of two isologous interfaces (Fig. 1A,D,G and Table 2). The larger interface is formed between two monomers that interact along flat β-sheets to form a dimer (Fig. S1E, Table 2, and Table S1). Apart from the numerous hydrophobic and H-bond interactions, the dimeric interface is also fortified by ~12 salt bridges. The calculated size of the interface (~2,300 $Å^2$) is somewhat underestimated because of a few unresolved loop segments – most notably a missing 13-amino acid-long fragment (positions 96–108) out of 28-amino acid-long flexible loop gating the access to the active site (positions 89–116) (Fig. S1A). The uMAT and eMAT dimers share a fairly similar topology (RMSD = 3.5 Å), supporting the notion that homodimerization along the large interface is highly conserved (Fig. S1C).

Comparison of eMAT structure with MAT from rat liver (rlMAT) reveals that, unlike the large dimeric interfaces, the smaller interdimeric interfaces of these structures are highly diverged. A relatively small solvent-accessible interaction core in rlMAT interface is contrasted by a much more extended interface in eMAT [2,23,24]. A substantially smaller (1,085 $Å^2$) isologous interdimeric interface facilitates the formation of the homotetramer via hydrophobic and H-bonds interactions. In contrary to the large interface, no salt bridges are being formed between

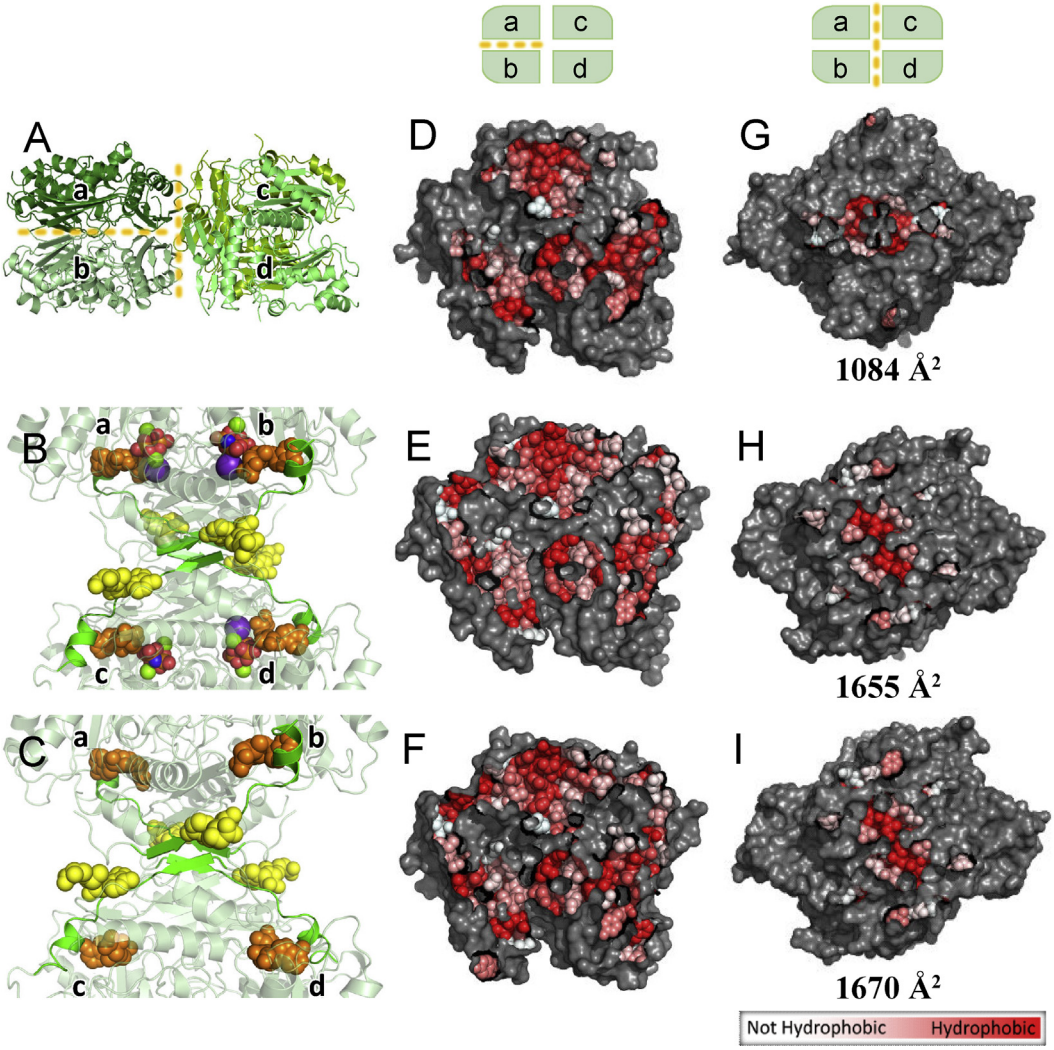

Fig. 1. SAM binds to the interdimeric interface of uMAT homotetramer. (A) Cartoon representation of uMAT crystal structure in the absence of ligands (PDB ID: 6RJS, 6RKC). See also Fig. S1. uMAT is a dihedral homotetramer formed along two isologous interfaces (shown in yellow dashed lines): Dimeric interface (between chains *a* and *b*, and between chains *c* and *d*) and interdimeric interface between dimers *ab* and *cd*. (B) Cartoon representation of uMAT crystal structure formed in the presence of AMPPNP and methionine (PDB ID: 6RKC). Four SAM molecules bind to each of the active sites (orange spheres), and four additional SAM molecules bind to the interdimeric interface (yellow spheres). Highlighted in green are the β-strands that participate in formation of continuous β-sheet passing through the interface, and flexible loops that adopt a closed state and lock the reaction products, SAM and PPNP, within the active sites. Potassium and magnesium ions are shown as purple and green spheres, respectively. Phosphate and nitrogen atoms of PPNP are shown as red and blue spheres, respectively. (C) Cartoon representation of uMAT crystal structure formed in the presence of SAM (PDB ID: 6RK7). The structure is identical to that shown in (B), with the exception of missing PPNP and metal ions. See also Fig. S5. (D, E, F) Surface representation of the dimeric interface (between chains *a* and *b*) of uMAT structures shown to the left. See also Table 2 and Table S1. Residues directly involved in protein-protein interactions are colored according to their hydrophobicity [51]. (G, H, I) Surface representation of the interdimeric interface (between dimers *ab* and *cd*) of uMAT structures shown to the left. The area of each interface is designated below (see also Table 2 and Table S1).

the dimers (Fig. 1G, Table 2 and Table S1). To validate that uMAT is a tetramer in solution, we performed analytical size exclusion chromatography coupled with multi-angle light scattering (SEC-MALS). At 100 μM (monomer concentration), a major peak of 163 kDa is observed, matching the anticipated molecular weight for uMAT tetramer (Fig. S2B). No dissociation is detected with dilution of the protein up to 12.5 μM (3.1 μM tetramer concentration), indicating that uMAT exists in solution predominantly in a tetrameric form at a low micromolar range (Fig. S2F).

Table 1. Crystallographic data collection and refinement statistics.

Structure	uMAT	uMAT	uMAT + AMP-PNP + methionine	uMAT + SAM	uMAT + SAM + ATP
PDB ID	6RJS	6RK5	6RKC	6RK7	6RKA
Data collection					
Beamline	ESRF ID30B	BL14.1 BESSYII	ESRF ID23-1	ESRF ID29	ESRF ID30B
Wavelength (Å)	0.972	0.9184	0.9780	0.9760	0.9762
Resolution range (Å)	47.62−2.6	47.6−2.6	47.78−2.6	48.66−1.8	46.62−2.50
Space group	P1	P21	P21	C21	I41
A, b, c (Å)	56.205, 64.064, 1114.495	56.358,80.450, 158.849	142.372, 79.467, 143.787	114.0, 106.14, 234.38	114.47, 114.47, 228.12
A, β, γ (°)	77.925, 83.855, 73.967	90.000, 94.463, 90.000	90.000, 105.107, 90.000	90.00, 96.86, 90.00	90.00, 90.00, 90.00
R-merge	0.098 (0.648)	0.099 (0.394)	0.076 (0.612)	0.033 (0.566)	0.105 (1.709)
R-meas	0.112 (0.746)	0.140 (0.558)	0.108 (0.866)	0.047 (0.800)	0.111 (1.811)
R-pim	0.055 (0.365)	0.099 (0.394)	0.076 (0.612)	0.039 (0.639)	0.037 (0.593)
CC1/2	0.997 (0.872)	0.984 (0.717)	0.996 (0.64)	0.996 (0.503)	0.999 (0.373)
Multiplicity	4.1 (4.0)	7.1 (7.2)	6.8 (6.2)	4.7 (4.2)	9.3 (9.2)
Completeness (%)	92.02 (87.26)	96.8 (98.0)	99.33 (97.96)	99.8 (99.6)	99.76 (98)
Mean I/sigma(I)	12.4 (2.25)	7.3 (1.9)	6.04 (1.15)	9.4 (0.9)	12.36 (0.92)
Refinement					
Reflections used in refinement	42413 (4040)	42299 (4259)	99706 (9755)	255430 (25309)	50369 (4946)
Reflections used for R-free	2044 (192)	2184 (207)	4986 (488)	12862 (1273)	2588 (251)
R-work/R-free	0.212/0.246	0.209/0.250	0.260/0.284	0.169/0.194	0.233/0.272
Number of nonhydrogen atoms	11399	11560	24088	19577	11679
Macromolecules	11316	11391	23838	18151	11601
Ligands			127	6	72
Solvent	83	169	123	1420	6
Protein residues	1440	1448	2982	2245	1470
Rmsd bonds (Å)	0.014	0.014	0.019	0.023	0.014
Rmsd angles (°)	1.94	1.95	2.16	2.13	1.89
Ramachandran favored (%)	94.66	96.37	96.33	97.4	94.65
Ramachandran allowed (%)	5.2	3.63	3.07	2.46	4.87
Ramachandran outliers (%)	0.14	0.00	0.61	0.13	0.48
Average B-factor	54.35	34.41	66.73	38.1	85.66
Macromolecules	54.48	34.66	66.88	37.78	85.48
Ligands			55.15	35.36	117.84
Solvent	35.77	17.32	50.85	42.14	57.83

Numbers in parentheses indicate statistics for the highest resolution shell.

Table 2. Interface size and composition analysis of orthologous MATs.

MAT (PDB ID)	Phylum/class	Monomer length[b]	% sequence identity to *E. coli*	Interface[c]	Δ^iG, kcal/mol[d]	Area[e]	# H-bonds[f]	# salt bridges[g]
E. coli (1P7L)	Proteobacteria/ gammaproteobacteria	384	100%	*large*	−22.2	2784	44	16
				small	−16.9	1743	8	4
M. tuberculosis (3TDE)	Actinobacteria/ actinobacteria	403	59%	*large*	−11.5	1983	23	11
				small	−13.8	1918	35	0
C. jejuny (4LE5)	Proteobacteria/ epsilonproteobacteria	398	41%	*large*	−21.3	2449	28	13
B. pseudomallei (3IML)	Proteobacteria/ betaproteobacteria	395	70%	*large*	−21.55	2103	26	11
				small	−8.4	950	8	0
N. gonorrhoeae (5T8S)	Proteobacteria/ betaproteobacteria	389	68%	*large*	−22.55	2642	43	17
				small	−4.7	1650	24	0
T. thermophiles (5H9U)	Deinococcus-thermus/ Deinococci	411	60%	*large*	−16.45	2441	30	15
				small	−18	1584	6	0
U. urealyticum (6RJS, 6RKC)[a]	Fermicutes/Mollicutes	376	44%	*large*	−17.35	2312	27	12
				small	−5.3	1084	10	0
U. urealyticum (AMPPNP + Met) (6RKC)[a]				*large*	−19.8	3069	49	14
				small	−6.7	1665	25	0
U. urealyticum (SAM) (6RK7)[a]				*large*	−22.9	3297	52	16
				small	−5.7	1670	24	0

[a] Structures solved in this work.
[b] Length of each MAT monomer in amino acids.
[c] Large interface is the dimeric interface between chains *a* and *b* or *c* and *d*. Small interface is the inter-dimeric interface between dimers (see Fig. 1 for chain annotation).
[d] The solvation free energy gain upon formation of the interface, in kcal/mol, as calculated by PISA server (see Materials and Methods). Negative $\boldsymbol{\Delta^iG}$ corresponds to hydrophobic interfaces and does not include the contribution of hydrogen bonds and salt bridges across the interface. The solvation free energy change of large interfaces is a mean of dimeric interfaces formed between chains *a* and *b*, and *c* and *d*. The $\boldsymbol{\Delta^iG}$ value obtained for small interfaces is a sum of 4 individual values calculated for the interactions between chains *a* and *c*, *b* and *d*, *a* and *d*, and *b* and *c*. See Table S1 for the individual values.
[e] Area — total interface surface area, in Å^2. Calculated by PISA server as difference in total accessible surface areas of isolated and interfacing structures divided by two. Area values for large and small interfaces were treated similarly to described in[d].
[f] Number of satisfied hydrogen bonds formed across the interface.
[g] Number of salt bridges formed across the interface.

Analysis of the available structures reveals that almost all bacterial MATs are dihedral homotetramers. Nonetheless, a dimeric MAT from *Campylobacter jejuni* (Table 2) is known, suggesting that the homotetramer has evolved by dimerization of the obligatory dimer. Indeed, it was suggested that the evolution of assembly of dihedral homotetramers proceeds via dimeric intermediates and is recapitulated *in vitro* by the (dis)assembly path of the complexes [8–10]. To uncover the (dis)assembly path of uMAT homotetramer, we first subjected the protein to native MS analysis (Fig. 2A). Three protein species, tetramer, dimer, and monomer, were found, suggesting that uMAT exists at equilibrium between these three states. Then, we subjected uMAT to an equilibrium unfolding in the presence of urea and monitored the unfolding effects using Trp fluorescence. Over 6 M urea range, a three-state unfolding landscape can be observed, with denaturation midpoint (C_m) of the first transition (between 0 and 3 M urea) equals 1.2 M and C_m of the second transition (between 3 and 6 M urea) equals 4.7 M (Fig. S2H). Analysis of the oligomeric species of uMAT formed in the presence of 0–2 M urea by SEC-MALS indicated tetramer-dimer dissociation, with approximately half of the species present in either tetrameric or dimeric state around 1 M urea (Fig. S2A–E). However, a third high-molecular-weight species was also present, in particular at and above 1.5 M urea, suggesting that dimeric and/or monomeric species are prone to aggregation. Collectively, these data indicate that uMAT follows tetramer-dimer-monomer assembly/disassembly path, as anticipated for a dihedral homotetramer.

SAM binds into the interdimeric interface of uMAT

The reaction catalyzed by MAT proceeds in two rather unusual steps [25]. First, sulfur of methionine attacks C5′ of ATP, producing SAM and triphosphate (PPP_i). In the second step, the bound triphosphate is hydrolyzed into P_i and PP_i, with P_i originating from the γ-phosphoryl group of ATP. When ATP is replaced with AMPPNP, the hydrolysis and release of PPP_i is almost completely blocked. In this case, the dissociation of SAM from the active site is extremely slow [26,27]. To reveal the structural effects of ligand binding, we solved uMAT crystal structure in the presence of AMPPNP and methionine at 2.6 Å and found that all four active sites of the homotetramer are occupied with SAM and PPNP (Fig. 1B, Table 1). In addition, the flexible loops (positions 89–116) – fully discernible in this structure – were found in a closed state, blocking the entrance to the active sites. The structural alignment of uMAT monomer with ordered flexible loop with its counterpart from eMAT reveals that the loop position is almost fully conserved in both structures (Fig. S1D). Furthermore, the orientation of SAM within the active sites of uMAT fully overlaps with SAM within the active sites of eMAT (Fig. S3A). Accordingly, all contacts between SAM and the active site residues appear fully conserved between MATs with known structures (Fig. 3A, Figs. S3B,C and S4A).

Although the addition of ligands did not prompt changes in the organization of the dimeric interface (with the exception of the contribution of the resolved active site loops, Fig. 1E, Table 2, and Table S1), we found profound changes in the interdimeric interface of the homotetramer (Fig. 1H, Table 2). First, in addition to the four SAM molecules occupying the active sites, four additional SAM molecules were found bound to the interdimeric interface (Fig. 1B). Second, dimers have rotated along the interface by ~45°. This rotation aligned the β-strands of the N-terminal domains into a continuous β-sheet running throughout the interface (Fig. 4) and increased the interface surface by almost 60% (from 1,084 $Å^2$ to 1,665 $Å^2$) (Fig. 1G and H, Table 2, and Table S1).

AMPPNP is not a physiological substrate, and the presence of nonhydrolyzable triphosphate in the active site could be partially responsible for the unusual properties of the obtained structure. To uncover the uMAT structural features under physiologically more relevant conditions, we solved uMAT crystal structure in the presence of SAM at 1.8 Å resolution (Fig. 1C,F,I and Table 1). The resulted structure was virtually identical to the structure obtained in the presence of AMPPNP and methionine: four SAM molecules bound to the active sites and sealed behind flexible loops and four additional SAM molecules bound to the interdimeric interface that rotated by ~45° (Fig. 4 and Fig. S5). (The only obvious difference between the structures is the presence of PPNP in association with two magnesium and one potassium ions in all four active sites, as shown in Fig. 1B.) Thus, the observed structural features are not a result of nonhydrolyzable PPNP.

SAM binding to the interdimeric interface locks flexible loops and inhibits catalysis

The conformational alternations of the flexible loops gating the access to the active sites (residues 89–116 in uMAT) are necessary to allow access of substrates and departure of products during the catalytic cycle and are directly linked to the catalytic turnover of MAT, as demonstrated for eMAT [28–30]. Analysis of uMAT structures reveals that binding of SAM molecules to the interdimeric interface is sterically possible only when flexible loops adopt a closed conformation (Fig. 3B–D, Fig. S4B). Indeed, in the absence of ligands, the loops are found in open conformations and pass through SAM-binding sites in the interdimeric interface. The side chain of Lys92, for instance, directly clashes with SAM, thus preventing

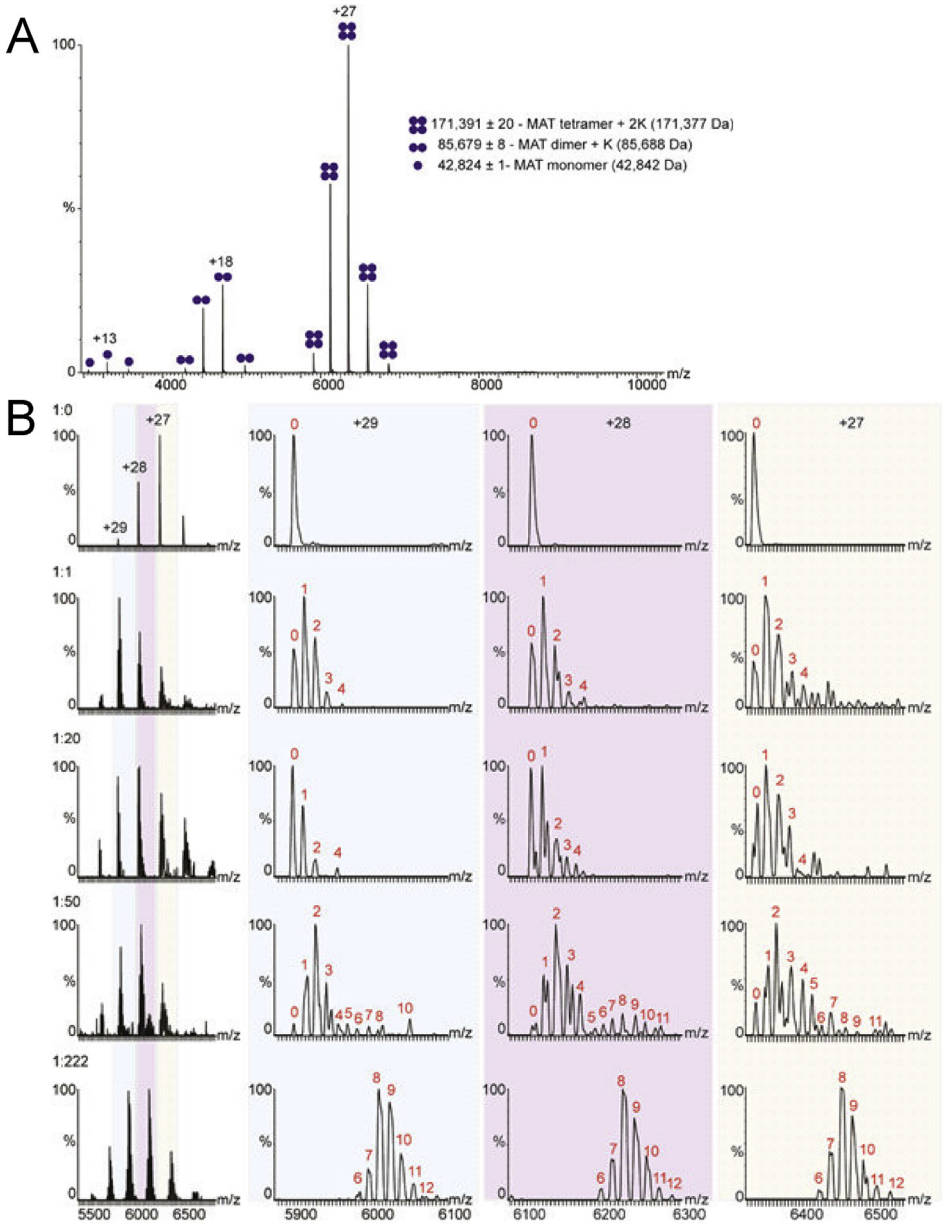

1:0 - MAT (9 μM)
171,391 ± 20 - T + 2K (171,376)

1:1 - MAT (9 μM) + SAM (9 μM)
171,388 ± 19 - T + 3K (171,416)
171,784 ± 7 - T + SAM + 2K (171,775)
172,173 ± 13 - T + 2SAM + 2K (1712,174)
172,651 ± 46 - T + 3SAM + 4K (172,651)
173,211 ± 32 - T + 4SAM + 8K (173,205)

1:20 - MAT (9 μM) + SAM (180 μM)
171,338 ± 21 - T + 2K (171,376)
171,522 ± 24 - T + 6K (171,533)
171,724 ± 13 - T + SAM + K (171,736)
172,250 ± 54 - T + 2SAM + 4K (172,252)
172,416 ± 53 - T + 2SAM + 8K (172,408)
172,632 ± 52 - T + 3SAM + 4K (172,651)
172,945 ± 24 - T + 4SAM + K (172,932)
173,164 ± 15 - T + 4SAM + 7K (173,166)

1:50 - MAT (9 μM) + SAM (450 μM)
171,400 ± 41 - T + 2K (171,416)
171,801 ± 25 - T + SAM + 3K (171,815)
171,915 ± 8 - T + SAM + 6K (171,932)
172,216 ± 36 - T + 2SAM + 3K (172,213)
172,585 ± 16 - T + 3SAM + 2K (173,572)
172,733 ± 43 - T + 3SAM + 6K (172,729)
173,061 ± 5 - T + 4SAM + 3K (173,049)
173,408 ± 23 - T + 5SAM + 3K (173,408)
174,192 ± 7 - T + 7SAM + 3K (174,205)
174,524 ± 25 - T + 8SAM + 1K (174,525)
174,692 ± 36 - T + 8SAM + 5K (174,682)
174,974 ± 22 - T + 9SAM + 2K (174,963)
175,315 ± 25 - T + 10SAM + K (175,322)
175,717 ± 12 - T + 11SAM + K (175,721)

1:222 - MAT (9 μM) + SAM (2 mM)
173,763 ± 20 - T + 6SAM + 2K (173,768)
174,185 ± 31 - T + 7SAM + 2K (174,166)
174,598 ± 21 - T + 8SAM + 3K (174,604)
175,026 ± 36 - T + 9SAM + 4K (175,041)
175,408 ± 30 - T + 10SAM + 3K (175,400)
175,862 ± 15 - T + 11SAM + 5K (175,877)
176,334 ± 39 - T + 12SAM + 6K (176,315)

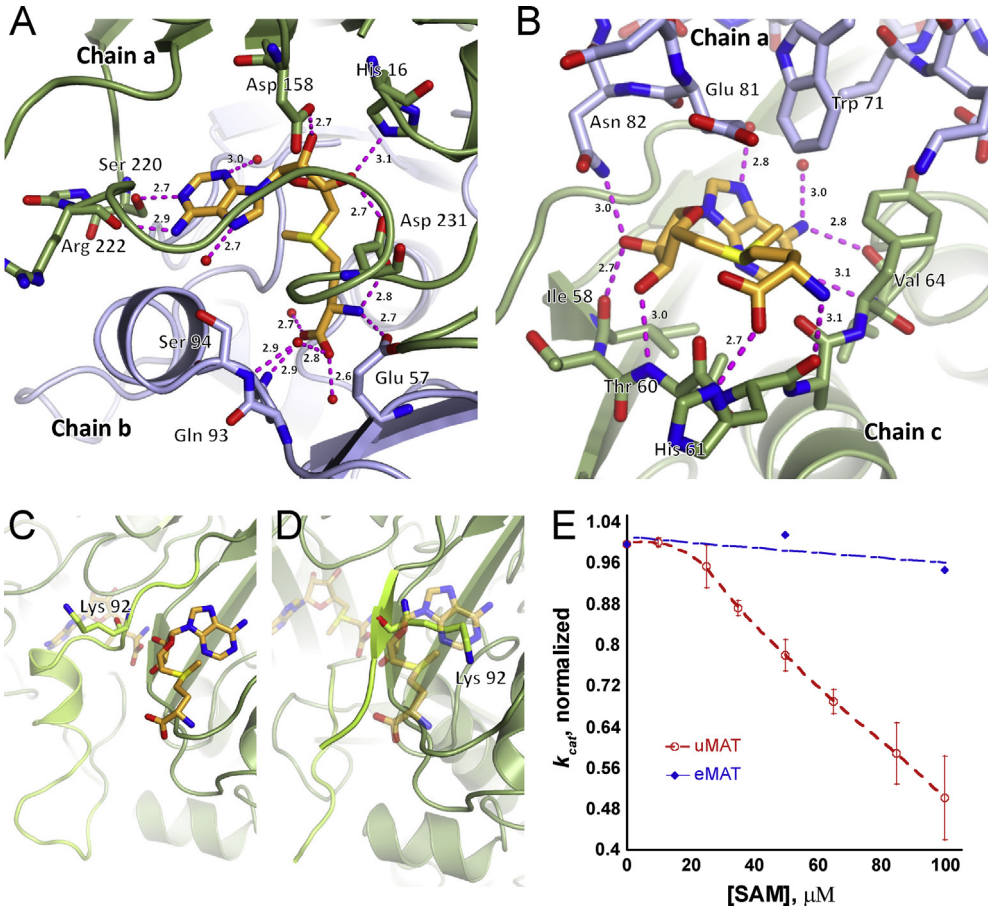

Fig. 3. SAM binding to the interdimeric interface locks the flexible loop in a closed state. (A) Active site of uMAT tetramer occupied with SAM (PDB ID: 6RK7). Chains a and b forming the active site pocket are presented as a cartoon. SAM molecule and uMAT residues forming direct interactions with SAM are shown as sticks (nitrogen, oxygen, and sulfur atoms are blue, red, and yellow, respectively). Red spheres represent water molecules, and dashed pink lines depict hydrogen bonds. The flexible loop (residues 89−116), shown in light green, adopts a closed conformation and locks SAM molecule within the active site (see also Fig. S3 and Fig. S4A). (B) Allosteric binding pocket of SAM in the interdimeric interface formed between chains a and c presented as sticks. SAM (shown in sticks) forms direct interactions with residues from both monomers. Water molecules and hydrogen bonds are marked as in (A) (see also Fig. S4B and Fig. S7). (C) SAM binding to the interdimeric interface is allowed when the flexible loop (light green) is closed. The faded SAM molecule in the background is occupying the active site. Note the orientation of side chain of Lys 92. (D) The overlay of uMAT structure obtained in the absence of ligands (6RJS) with SAM from the SAM-supplemented structure (6RK7) shows a steric hindrance that prevents SAM binding to the interface when the flexible loop (shown in light green) is open. Note the orientation of the side chain of Lys92 that directly clashes with SAM molecule. (E) The catalytic turnover (k_{cat}) of uMAT (shown in red) is highly sensitive to SAM concentration. Under the identical conditions, the catalytic turnover of eMAT (blue) is only slightly affected. Error bars represent standard deviation between three independent measurements. See also Fig. S6.

Fig. 2. Electrospray native-state MS analysis of uMAT. (A) uMAT protein exists in equilibrium between tetramers, dimers, and monomers. Mass measurements indicate that the dimer and tetramer are bound to potassium ions (K^+). Values in brackets show the theoretical masses of the different protein species.(B) The stoichiometry of binding between uMAT and SAM measured by native-state MS. uMAT spectra are shown on the left, and the enlargement of 3 consecutive charge states (+29, +28, +27) is shown on the right. uMAT/SAM molar ratios are indicated on the left side of each tetramer spectrum. The resulting spectra, which are mostly baseline resolved, reveal a clear distribution of peaks corresponding to an ensemble of MAT tetramers bound to an increasing number of SAM molecules and potassium ions. The fine structure of each charge state is a result of the combination of peaks that correspond in mass to different numbers of bound SAM molecules, which are indicated in red. Measured masses of the different species in each experiment are listed under figure. T, tetramer; K, potassium.

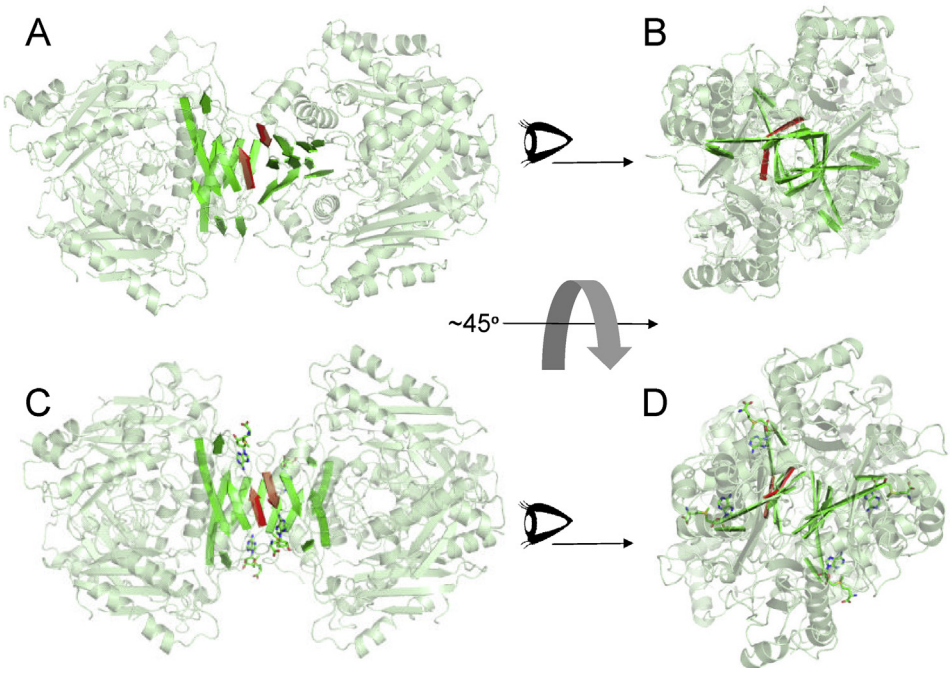

Fig. 4. SAM binding to the interdimeric interface is accompanied by structural rearrangement of uMAT tetramer. (A) Position of β-strands (colored in red and green) running through the interdimeric interface of uMAT obtained in the absence of ligands (PDB ID: 6RK7). (B) Back view of the structure shown in (A). (C) When SAM (shown in sticks) is bound to the interdimeric interface, dimers rotate by ~45°, resulting in formation of a continuous β-sheet that stiches both dimers together (PDB ID: 6RK7). Note the shift in the position of red β-strands. (D) Back view of the structure shown in (C).

its binding to the interface when the loop is open (Fig. 3C and D). Conversely, the presence of SAM in the active site appears to facilitate loop closure, thus exposing the binding site in the interdimeric interface for an additional SAM molecule. This is achieved by a direct hydrogen bond formation between amine moiety of Gln93 side chain of the loop and carboxyl moiety of the active site bound SAM (Fig. 3A, Figs. S3B and S4A). The adjacent Ser94 also forms a hydrogen bond with a water molecule engaged in additional hydrogen bond with the same carboxyl group of SAM (Fig. 3A, Figs. S3B and S4A).

To link this previously unknown mode of interface SAM binding to the catalytic activity of uMAT, we measured uMAT enzymatic activity in the presence and absence of SAM. In the absence of SAM and at a limiting concentration of ATP and saturated amounts of Met, and, conversely, at a limiting concentration of Met and saturated amounts of ATP, we measured the following kinetic parameters: k_{cat} = ~0.5 sec^{-1} (per active site), $K_{m(ATP)}$ = 106 μM, and $K_{m(Met)}$ = 51 μM (Fig. S6). These values are very close to the kinetic constants reported for eMAT [27,30]. However, when the enzymatic reaction was conducted at saturated amounts of both ATP and Met (*i.e.*, the reaction proceeded at V_{max}), addition of SAM to the reaction mix produced a severe reduction in the catalytic turnover (~50% reduction in k_{cat} in presence of 100 μM SAM, Fig. 3E). In sharp contrast, addition of SAM to eMAT under identical conditions did not produce a significant reduction in k_{cat} (Fig. 3E). This finding is readily explained by the structural rearrangement induced by SAM in uMAT: An increase in SAM concentration leads to locking the active site loops, movements of which are essential for the catalytic turnover.

SAM binding to the interdimeric interface involves interactions with monomers from both dimers

What is the nature of the interactions formed by SAM molecules within the interdimeric interface? We found that SAM-binding pockets are laid with strong negative charge, which might facilitate the electrostatic interactions with the positively charged sulfonium ion of SAM (Fig. S7A). Furthermore, each of the SAM molecules in the interdimeric interface forms interactions with monomers from both dimers, thus reinforcing the integrity of the tetrameric complex (Fig. 3B). For example, one of the hydroxyl groups of ribose forms hydrogen bonds with the backbone carbonyl of I58 from monomer *c* and side chain carboxyl of N82 from the opposite monomer, *a*. The adenine moiety also interacts with both monomers. While the C-6 amino group of adenine is stabilized by hydrogen bonds formed with backbone of V64 (monomer *c*), W71 from

monomer *a* flips to form T-shaped π-stacking interaction with adenine ring (Fig. 5A; see also Fig. 3B). Accordingly, in solution, addition of SAM is accompanied by a reduction in Trp fluorescence, whereas binding of ATP to the active site is not accompanied by a fluorescence change (Fig. 5B). This suggests that the drop in Trp fluorescence upon SAM addition is predominantly originating from the shift in W71 orientation in the interface.

We could thus use Trp fluorescence to measure the effect of SAM binding on the kinetics of uMAT tetramer dissociation. To this end, we mixed uMAT with 3 M urea in a stopped-flow apparatus and monitored the pre−steady-state dissociation kinetics with Trp fluorescence. This particular concentration of urea was chosen, because, as demonstrated previously with equilibrium unfolding of uMAT in presence of urea, at 3 M urea tetrameric and dimeric species of uMAT are fully dissociated, yet the monomeric species has not yet undergone unfolding (Fig. S2). In the absence of ligands, mixing of uMAT with 3 M urea resulted in a rapid drop in Trp fluorescence (Fig. 5C). Fitting the trace to a sum of two exponentials produced an observed rate constant k_{obs} ~0.15sec^{-1} for the first exponential. The value of the observed rate constant for the second exponential was an order of magnitude lower (Fig. 5C). Addition of ATP did not affect the dissociation kinetics (Fig. 5C). However, in the presence of SAM, two important changes were observed (Fig. 5D). First, a drop in Trp fluorescence was preceded by a rapid trace of ~2 s, during which Trp fluorescence has increased. Because association of SAM with the interface is accompanied by a drop in Trp fluorescence (Fig. 5B), we interpret the rise in Trp fluorescence to be a result of SAM dissociation from the interface. Importantly, an equimolar amount of ATP did not produce any significant change in the onset of the kinetic trace comparatively to that obtained in the

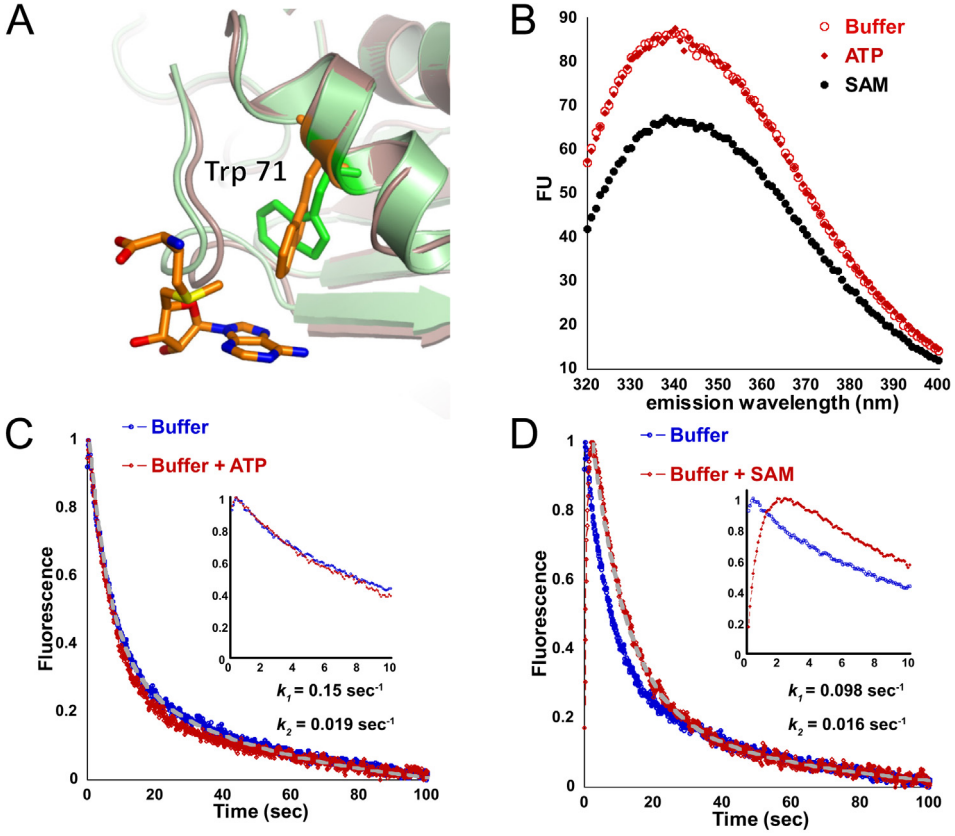

Fig. 5. SAM binding to the interdimeric interface delays the rate of uMAT tetramer dissociation. (A) Structural alignment between uMAT monomer in the absence (green, PDB ID: 6RK7) and presence (brown, PDB ID: 6RK7) of SAM shows a shift in the orientation of W71. SAM molecule in the interface is depicted as sticks. See also Fig. 3B. (B) Steady-state tryptophan fluorescence measurement of uMAT in the absence (empty red circles) and presence of ATP (red diamonds) or SAM (black closed circles). Binding of SAM is accompanied by a substantial drop in Trp fluorescence. (C, D) Kinetics of uMAT urea-induced unfolding monitored by a shift in Trp fluorescence in the absence (blue trace) and presence of ATP [red trace, (C)] or SAM [red trace, (D)]. The kinetic traces were fitted to a sum of two exponentials (see Materials and Methods). Insets show the kinetic traces within the first 10 s. In the presence of SAM, the kinetics of uMAT tetramer dissociation is markedly delayed.

absence of ligands (Fig. 5C). Second, fitting the trace of the delayed drop in Trp fluorescence to a sum of two exponentials shows ~30% reduction in the observed rate constant of the first exponential (k_{obs} ~ 0.1sec^{-1}), while the value of the second exponential remained unchanged (Fig. 5D). These data suggest that binding of SAM molecules to the interdimeric interface increases the kinetic stability (*i.e.*, decreases the rate of dissociation) of uMAT tetramer.

SAM binding preserves the integrity of the homotetrameric complex

To further explore the effect of SAM binding on stability of uMAT tetramer, we used bis-ANS (4,4'-Dianilino-1,1'-Binaphthyl-5,5'-Disulfonic Acid, Dipotassium Salt) – a probe for surface hydrophobicity and folding intermediates [31–33]. Fig. 6A shows that addition of both ATP and SAM prompted a substantial reduction in bis-ANS fluorescence at a steady state, indicating a tighter packing of the protein upon ligand binding. However, the effect of SAM on the reduction of bis-ANS fluorescence was much more pronounced than that of ATP. This difference is expected because ATP, unlike SAM, is not supposed to bind to the interface and is therefore unable to trigger the realignment of the dimers and block solvent exposure of the interface.

Then, we used a fluorescence thermal shift assay to follow thermal unfolding of uMAT in a high-throughput manner. To make the assay compatible with a real-time polymerase chain reaction (PCR) detection system, we replaced bis-ANS with SYPRO-orange dye (see Materials and Methods and refer to the study by Chari et al [34], Ericsson et al [35], and Lavinder et al [36]). We validated that replacement of bis-ANS with SYPRO-orange indeed produces a pattern of reduction in uMAT fluorescence in the presence of SAM or ATP similar to that obtained with bis-ANS (Fig. S8A). We followed the thermal unfolding of uMAT at a range of 20 °C–90 °C (Materials and Methods). Two distinct transitions can be observed in the absence of ligands (Fig. 6B). The thermal midpoint (T_m) of the second transition (~50 °C) coincides with T_m obtained for thermal unfolding monitored by Trp fluorescence, suggesting that the second transition reports the unfolding of monomeric species (Fig. 6D and Fig. S8B). The much lower T_m of the first transition (~30 °C) suggests that it reports on the integrity of the tetramer (order/disorder of the active site loops, and accessibility of the interdimeric interface). The addition of AMPPNP and Met has completely erased the first transition (Fig. 6C). A similar effect was observed during urea equilibrium unfolding of uMAT in the presence of AMPPNP and methionine (Fig. S2G,I). This behavior is expected because production of SAM and PPNP drastically transforms the structural organization of the tetramer: All active site loops are ordered, and the access to the interdimer interface is blocked by four SAM molecules. Because SAM and PPNP cannot freely dissociate from the active sites, their presence also shifts the T_m of the second transition (monomer unfolding) by ~5 °C (Fig. 6D). When added separately, Met and AMPPNP (1 mM each) has no measurable effect on the second transition (Fig. 6D). AMPPNP (but not Met), however, has a mild stabilizing effect (T_m increases by ~2 °C) on the first transition (Fig. 6C). The effect of ATP addition was almost identical to that of AMPPNP. In contrast, addition of the equimolar amount of SAM had a profound effect on the first transition (T_m increased by > 10 °C), without having any measurable impact on the second transition (Fig. 6C and D). At a range of 0–2 mM SAM, the T_m of the first transition has shifted by > 17 °C. The same concentration range of ATP produced only 4 °C increase in T_m (Fig. 6E), indicating that SAM has a profoundly more powerful impact on the integrity of uMAT homotetramer than the effect of ATP.

The data presented so far indicate that addition of SAM molecules to uMAT tetramer causes unique structural rearrangement in the tetramer configuration, manifested in highly compact and kinetically stable structure. What is the possible physiological role of SAM-induced kinetic stabilization of uMAT tetramer? It was demonstrated that the kinetic stability of proteins is tightly linked to their ability to withstand proteolysis [37]. We thus compared the sensitivity of uMAT and eMAT to proteolysis by trypsin and thermolysin in the presence and absence of SAM. While no change in eMAT sensitivity to proteolysis was observed, strikingly, addition of SAM practically blocked uMAT degradation by both proteases (Fig. 6F). The fact that the structural rearrangement of uMAT tetramer caused by the elevated SAM levels decreases its degradation propensity suggests that SAM levels control uMAT half-life *in vivo*.

SAM binding triggers multiple structural rearrangements of uMAT

Crystal structures of uMAT, which we solved in the absence and presence of ligands, indicate two distinct homotetrameric states. However, multiple structural rearrangements are required to cross between these states, including closure of the flexible loops, realignment of dimers, and binding of two SAM molecules per each monomer. Although SAM binding to the interface is sterically blocked when the flexible loop is open, no steric hindrance prevents its binding before structural rearrangement of the dimers, further increasing the number of possible structurally distinct conformations existing between these two states (Fig. S7B). Collectively, these features suggest that in solution, an equilibrium between multiple structurally distinct states

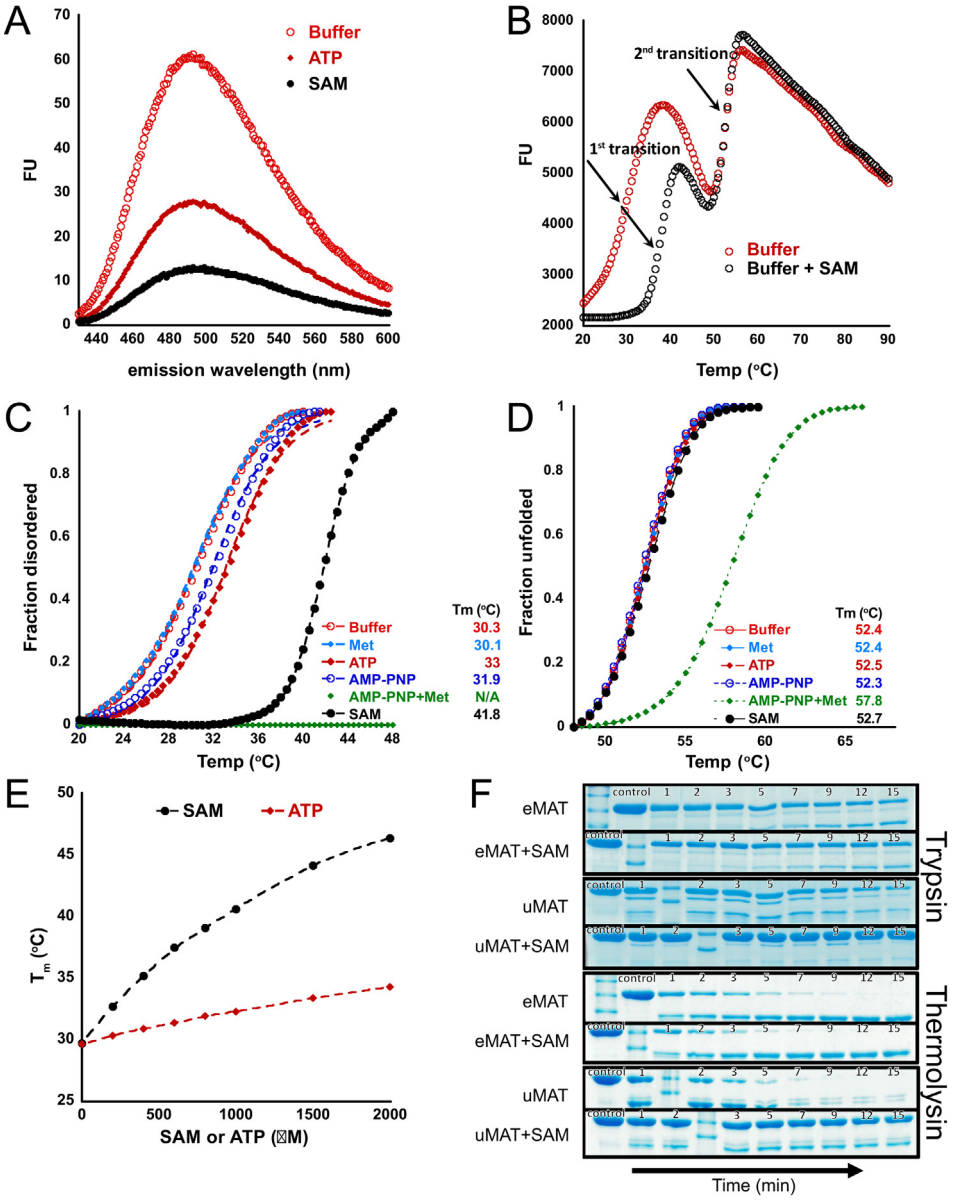

Fig. 6. SAM binding stabilizes uMAT tetramer and renders it resistant to proteolysis. (A) Steady-state bis-ANS fluorescence measurements of uMAT in the absence (open red circles) and presence of ATP (red diamonds) or SAM (closed black circles). See also Fig. S8. (B) SYPRO-orange thermal unfolding of uMAT in the presence (open black circles) and absence (open red circles) of SAM shows that SAM affects the first of the two thermal transitions. (C) Normalized data for the first transition of thermal unfolding show that SAM (black closed circles) has a great stabilizing effect, while a combination of AMPPNP and methionine (green diamonds) fully erases the first transition. To derive the thermal midpoint (T_m) values, the data were fit to a two-state model (see Materials and Methods). (D) Normalized data for the second transition of thermal unfolding show that a combination of AMPPNP and methionine is the only condition affecting the transition. T_m values were derived as in C. (E) A correlation between shifts in T_m values of the first transition and SAM (black circles) or ATP (red diamonds) concentrations. The effect of SAM on the first transition is profound. (F) Trypsin and thermolysin proteolysis of uMAT and eMAT in the absence and presence of SAM (see Materials and Methods). Addition of SAM has a profound impact on uMAT resistance to proteolysis, while addition of SAM provides no protection from degradation of eMAT.

should exist at a given concentration of SAM. To test this conjecture, we explored the stoichiometry of SAM binding to uMAT using native state MS (Materials and Methods). The results show that up to a 20-fold molar excess of SAM, the uMAT tetramer associates with up to 4 molecules of SAM. However, in the presence of increasing SAM concentrations, a step-wise shift of SAM binding to uMAT is observed

(Fig. 2B). At the highest measured ratio (1:200), the entire population of uMAT shifts toward binding of 6–12 molecules of SAM, suggesting positive cooperativity in SAM binding. (The binding of higher than 8 molecules of SAM to the tetramer is attributed to nonspecific binding, which is a known drawback of the electrospray ionization method [38].)

The complex dynamics described previously is probably further complicated in the living cell because of competition between SAM and ATP for binding to the active sites. In an attempt to understand the effects of ATP/SAM competition, we solved a crystal structure of uMAT in the presence of both ligands at 2.5 Å resolution (Fig. S1E, Table 1). We found that addition of both ligands does not trigger structural rearrangement of uMAT tetramer. The large interface of this structure is identical to the large interfaces of all other uMAT structures (Fig. S1F, Table 2 and Table S1), whereas the small interface is identical to that determined for uMAT in the absence of ligands (Fig. S1G, Table 2 and Table S1). The active site of chain *a* showed electron-density map of both ATP and SAM, revealing that the obtained crystal structure, in fact, reports an ensemble of states. However, it is noteworthy that the flexible loop gating the active site (positions 96–108) was resolved only when SAM is present in the active site (chains *a* and *c*, Fig. S1E). ATP alone was not sufficient to prompt the closure of the loop (chain *b*, Fig. S1E). These features hint to the possibility that there is a kinetic barrier to reach the structural rearrangement of uMAT tetramer: Unless all loops are closed, the dimers cannot realign along the interdimeric interface and reach a more stable configuration with markedly increased interface surface area. Reaching this state is possibly the reason for an apparently cooperative SAM binding detected by native state MS (Fig. 2B). Because the presence of ATP in the active site does not constrain the movement of the flexible loops, it is plausible that when ATP outcompete SAM in the active site, SAM binding to the interdimeric interface is hindered. It follows that ATP/SAM ratio, rather than SAM alone, controls the structural rearrangement of uMAT tetramer *in vivo*.

The interdimeric interface of MATs is an adaptive hotspot

To better understand the possible adaptive role of the interdimeric interface in MATs, we analyzed both isologous interfaces of bacterial MATs with available structures (Fig. 7, Table 2 and Table S1). We found that the residue composition and geometric patterns of the large interface is highly conserved in all MAT structures. This conservation is also manifested in the fact that the surface area of the large interface significantly correlates with the number of H-bonds, which is a general feature of protein interfaces [39] (Fig. S9A, Table 2 and Table S1). Conservation of the large dimeric interface holds despite the fact that bacterial species within which the MAT proteins resign occupy highly distinct ecological niches, including disease-causing parasitizing bacteria (*Neisseria gonorrhoeae* and *U. urealiticum*) and thermophilic bacterium *Thermus thermophiles*. This finding suggests that the evolution of the large interface is predominantly constrained by the enzymatic activity of uMAT. In sharp contrast, the residue composition, geometric patterns, and the surface area of the inter-dimeric interfaces appear highly diverged (Fig. S9, Table 2 and Table S1). For example, *E. coli* is the only species among the analyzed MATs, the interdimeric interface of which is fortified with salt bridges. Furthermore, the amount of H-bonds in the interdimeric interface does not correlate with the surface area, largely because of the deviation of *E. coli* and *T. Thermophiles* MATs from the general trend (Fig. S9B). Overall, these findings support the hypothesis that by acting on the interdimeric interface, evolution preserves the enzymatic activity of MATs, while tailoring its other molecular properties, such as the intracellular protein turnover or regulation of activity in response to metabolite levels, to the unique needs of the organism via the tetramer.

Discussion

Cellular proteomes are dominated by symmetric homomeric structures [8,40–42], with dihedral homotetramers (dimers of dimers) being the second most abundant symmetry group enriched with metabolic enzymes [8,22,40]. It was suggested that the evolution of assembly of dihedral homotetramers has proceeded via dimeric intermediates [43]. However, because the evolutionary more ancient dimeric configurations must already have been functional, the adaptive role of homotetramerization is not obvious, especially, given the fact that, as is the case with MAT, dihedral homotetramers often have functional dimeric orthologs. Here, we address the functionality associated with homotetramerization of MAT from *U. urealiticum*, a dihedral homotetramer, whose crystal structure we solved in the absence and presence of ligands. We show that the evolutionary more recent interdimeric interface has evolved to control the enzymatic activity that takes place in the ancient and highly conserved dimeric interface in response to product accumulation. Specifically, the interdimeric interface accommodates four allosteric SAM binding sites (one per each monomer). Binding of SAM molecules to the interface is associated with profound structural rearrangements of the entire uMAT tetramer. First, flexible loops gating the access to the active sites remain locked in the closed conformation, thus inhibiting the catalytic turnover. Second, the

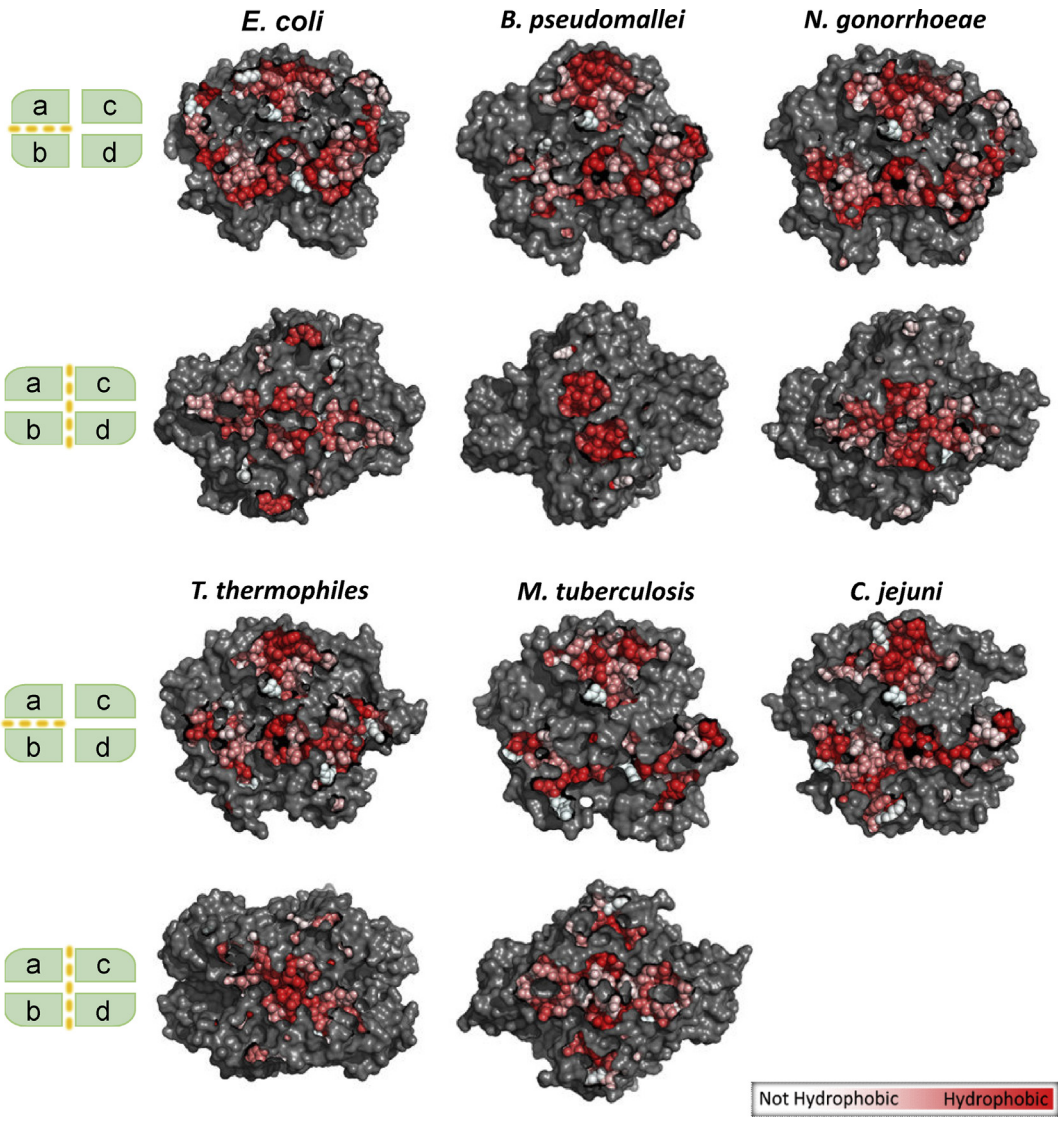

Fig. 7. Comparison of large and small interfaces in bacterial MATs with known structures. Surface representation of dimeric (between chains a and b) and interdimeric (between dimers ab and cd) interfaces. Residues directly involved in protein-protein interactions are colored according to their hydrophobicity [51]. (See also Table 2 and Table S1). Note the high conservation among large interfaces and high divergence among small ones. See also Fig. S9.

dimers rotate along the interdimeric interface, causing ~60% increase in the surface area and formation of a continuous β-strand that passes through the interface. Binding of four SAM molecules to the interdimeric interface therefore seals the interface from solvent exposure. Together, these structural rearrangements render the entire homotetramer kinetically stable, a property manifested in the markedly decreased sensitivity to proteolysis.

Importantly, neither the allosteric regulation of catalytic activity nor the increased stability of the tetramer in response to SAM accumulation has been reported in other MATs. Mapping the residues directly interacting with SAM in the interdimeric interface of uMAT on multiple sequence alignment comprised of bacterial MATs suggests that other Mollicutes, *e.g.*, *Mycoplasma pneumonia*, might possess a similar regulation mode (Fig. 3B and Fig. S9C). Why did *U. urealiticum* and, possibly, other Mollicutes evolve this unique mode of regulation? Evolution of Mollicutes was accompanied by massive genome reduction that resulted in reduced metabolic capacity and absence of effectively functioning transcriptional regulation [44–46]. For instance, methionine metabolism is tightly regulated by a network of transcription factors and metabolites (including SAM) in *E. coli* [47]. This type of regulation is completely missing in *U. urealiticum* that possesses neither genes involved in *de novo* methionine synthesis nor transcription factors needed for its regulation. The paucity of transcriptional regulation of

metabolism in Mollicutes could have resulted in "delegating" the regulation of MAT activity directly to the protein level. In addition, many Mollicutes, including *U. urealiticum*, have lost GroEL/ES chaperonins but preserved AAA + ATP-dependent proteases, such as Lon [48,49]. This prompted the idea that proteostasis in Mollicutes might be skewed toward protein degradation [48]. Accordingly, the increased stability of uMAT tetramer in the presence of saturating amounts of SAM might be an adaptive feature that prevents its degradation *in vivo*.

The regulation of uMAT activity and stability via SAM binding to the interdimeric interface of the tetramer is obviously a functionally beneficial result of selection operating on the interface. Analysis of the interfaces of other bacterial MATs with known structures reveals a sharp contrast in the evolutionary preservation of the dimeric versus the interdimeric interfaces. While the larger and evolutionary ancient dimeric interface preserves residue composition, types of contacts, and surface geometry across MATs originating from bacteria that occupy distinct ecological niches, the smaller and evolutionary recent interdimeric interface exhibit highly diverged surface geometries, residue composition, and nature of contacts within the interface. For instance, the interdimeric interface of MAT from *T. thermophiles* has a relatively low number of hydrogen bonds (only 6 per surface of 1584 $Å^2$) and also the highest number of hydrophobic contacts among all bacterial MATs, manifested in the lowest solvation energy per 1 $Å^2$ of the interdimeric interface (Table 2). Because hydrophobic packing is the major contributing factor to stabilization of thermophilic proteins [50], highly dense network of hydrophobic interactions in the interdimeric interface is likely an adaptation to thermophilic lifestyle. Based on this analysis, we propose that, while the evolutionarily ancient and highly conserved dimeric interface of MAT controls its primary enzymatic function and the assembly path of the tetramer, the more recent interdimeric interface is recruited by evolution to tune the molecular properties of the entire tetramer and tailor them to the specific needs of the organism. Finally, the existence of the homomer-level modes of regulation of stability and activity that stems from the evolutionary tinkering of the interdimeric interface also provides a clue as to why dihedral homomers exhibit a particularly strong functional enrichment in metabolic enzymes [22].

Materials and Methods

Gene cloning, protein expression, and purification

The gene encoding uMAT was custom synthesized by Integrated DNA Technologies with a fused fragment encoding C-terminal Hisx6 tag and flanking NdeI and XhoI restriction sites. To this end, the protein sequence of uMAT (NCBI reference sequence WP_004025944.1) was converted to DNA sequence using the manufacturer's *E. coli* codon optimization tool. The gene encoding eMAT was amplified directly from the chromosome of *E. coli* MG1655 using the following primers: For: CATATGGCAAAACACCTTTTTACGTCC-GAGTCCGTCTC and Rev: CTCGAGCTAT-TAATGGTGATGGTGATGGTGCTTCAGACCGG-CAGCATCGCGCAGCAGCTGCGCTTTG. The For primer introduces NdeI restriction site. The Rev primer introduces a fused fragment encoding C-terminal Hisx6 and XhoI restriction site. Both genes were cloned into pET24a expression system using NdeI/XhoI restriction sites and expressed in BL21(DE3) cells. Specifically, an overnight starter was diluted 1:100, grown at 37 °C until OD at 600 nm was 0.5, after which the expression was induced by the addition of 0.4 mM IPTG overnight at 30 °C. Cells were centrifuged at 4800×*g*, and the pellet was stored at −20 °C. Cells were lysed by sonication after a 30-min preincubation with 1 mg/ml lysozyme (Sigma) and 500U benzonase (Sigma) on ice. The filtered lysate was purified by Ni-NTA on a His-TRAP FF 5-ml column (GE Healthcare) and dialyzed into 25 mM Tris pH 8.0, 150 mM KCl, 1 mM DTT. This was followed by size-exclusion chromatography (monitored at 280 nm) on a Superdex 200 16/600 column (GE Healthcare) in the same buffer. uMAT fractions were dialyzed against 20 mM MOPS-KOH pH 7.5, 10 mM KCl, 1 mM DTT, while eMAT fractions were not subjected to buffer exchange. The proteins were concentrated using Amicon centrifugal filters and stored at 4 °C. Protein purity was validated by sodium dodecyl sulfate−polyacrylamide gel electrophoresis (SDS-PAGE) analysis (Fig. S10).

Protein crystallization, data collection, structure determination, and refinement

uMAT structure in the absence of ligands (PDB ID: 6RJS): Five mg/ml of uMAT protein was mixed 1:1 (v/v) with reservoir solution and crystallized by the sitting drop method over a reservoir containing 5% Tacsimate, 0.1 M Hepes pH 7.0, and 10% polyethylene flycol (PEG) 5 K at room temperature. *uMAT structure in the absence of ligands (PDB ID: 6RK5):* 10 mg/ml uMAT was mixed 1:1 (v/v) with reservoir solution and crystallized by the sitting drop method over a reservoir containing 0.2 M $MgCl_2$, 0.1 M Hepes pH 7.4, and 20% PEG 3350 at room temperature. *uMAT structure in the presence of AMPPNP and methionine (PDB ID:* 6RKC*)*:10 mg/ml uMAT with 5 mM AMPPNP and 5 mM methionine was mixed 1:1 (v/v) with reservoir solution and crystallized by the sitting drop method over a reservoir containing 0.1 M magnesium formate and

12% PEG 3350, at room temperature. *uMAT structure in the presence of SAM (PDB ID: 6RK7):* SAM was purchased from Sigma (A7007); 20 mM SAM solution was prepared in 10 mM H_2SO_4, flash frozen, aliquoted, and stored −20 °C. Ten mg/ml uMAT with 1 mM SAM was mixed 1:1 (v/v) with reservoir solution and crystallized by the sitting drop method over a reservoir containing 0.1 M Hepes pH 7.0 and 30% Jeffamine ED-2001 at room temperature. *uMAT structure in the presence of ATP and SAM (PDB ID: 6RKA):* Ten mg/ml uMAT with 4 mM ATP and 2 mM SAM was mixed 1:1 (v/v) with reservoir solution and crystallized by the sitting drop method over a reservoir containing 0.2 m Li2SO4, 0.1 M Tris pH 8.5 and 25% PEG 3350 at room temperature.

Crystals were harvested, cryoprotected, and flash-cooled in liquid N_2. X-ray diffraction data were collected at beamline ID30B of the European Synchrotron Radiation Facility (ESRF, Grenoble, France). Data were collected at 100 K from one crystal of uMAT that diffracted to 2.6 Å resolution. The crystal belongs to the space group P1, with unit cell dimensions of a 56.205, b 64.064, and c 114.495, and it contains four copies of the protein in the asymmetric unit. X-ray data were merged and scaled by X-ray diffraction spectroscopy (XDS) [52] and was solved by molecular replacement using Phaser [53] in CCP4 [54]. Native monomer of eMAT (PDB ID: 1FUG) was used as a search model. Refinement used alternating cycles of manual rebuilding in COOT [55] and automated refinement using Refmac5 [56]. The coordinates and structure factors have been submitted to the PDB under the accession code 6RJS.

Ligand omit map construction (*Fo-Fc*)

Ligand omit maps were constructed using Phenix 1.16−3549 (https://www.phenix-online.org/). Maps were then converted to a.map format using CCP4, followed by a manual conversion to a.map.ccp4 format. These files were then visualized using PyMOL.

Enzymatic activity

uMAT activity was determined at 37 °C in activity buffer (25 mM Hepes pH 7.5, 100 mM KCl, 10 mM $MgCl_2$, 1 mM DTT) at either a saturated concentration of methionine (5 mM) and a range of ATP concentrations (0−500 μM) or at a saturated amount of ATP (5 mM) and a range of methionine concentrations (0−500 μM). uMAT (100 nM) was preincubated with 5 mM of either ATP or methionine at room temperature for 30 min. The enzymatic reaction was initiated by adding either ATP or methionine. Aliquots were removed from the reaction mix at various time points, and the reaction was stopped by mixing with 10% perchloric acid in a 1:1 ratio. The aliquots were then centrifuged, and the supernatant was separated by high-performance liquid chromatography (HPLC) using the MultiHigh SCX 5μ 250 × 4.6 mm column (CS-Chromatographie Service GmbH). The mobile phase consisted of 400 mM ammonium fumarate (adjusted to pH 4.0 using formic acid) at a flow rate of 1 ml/min, while measuring absorbance at 254 nm. Data analysis was performed by integrating the peaks corresponding to SAM and fitting them to a calibration curve (Fig. S6A,B). The kinetic constants were derived by fitting the resulted data point to a Michaelis-Menten equation (V_{max}•[S]/K_m+[S]) (Fig. S6C,D).

To measure the inhibitory effect of the reaction product on uMAT and eMAT, enzymes (100 nM) were preincubated with 5 mM methionine and a range of SAM concentrations (0−100 μM). The reaction was initiated by adding 1 mM ATP. Because at these highly saturated concentrations of substrates, the reactions catalyzed by both eMAT and uMAT proceed at maximal speed, we treated the linear slopes of the initial velocities obtained at each concentration of SAM as V_{max}. The catalytic turnover numbers (k_{cat}) were derived by dividing the maximal velocity values by total enzyme concentrations (Fig. 3E).

Analytical SEC-MALS

Multiangle light scattering (MALS) analysis on MiniDawn TREOS + OPTILAB T-reX (WYATT) was performed to determine the molecular weight of uMAT species separated by size-exclusion chromatography (SAM) on AKTA Pure M25 (GE). uMAT samples were incubated for 24 h at room temperature in 20 mM MOPS-KOH pH 7.5, 10 mM KCl, 1 mM DTT at different protein concentrations (12.5−200 μM, monomer concentration), or at 100 μM in the presence of a range of urea concentrations (0−6 M). The samples were then injected into a Superdex 200 Increase 30 × 1cm column equilibrated with 25 mM Tris-HCl pH 8.0, 150 mM KCl, 1 mM DTT, and the corresponding urea concentration.

Urea equilibrium unfolding experiments

uMAT samples (2 μM each) were prepared in 20 mM MOPS-KOH pH 7.5, 10 mM KCl, 1 mM DTT, and 10 mM $MgCl_2$ at a range of urea concentrations (0−6 M) in the absence of ligands or in the presence of either 1 mM SAM or 1 mM of each AMPPNP and methionine. The samples were incubated for 24 h at room temperature, and their tryptophan fluorescence (ex. 295 nm, em. spectrum 320−400 nm) was obtained using Cary Eclipse fluorescent spectrophotometer (Agilent). To account for the shifts in fluorescence, the spectra were analyzed

as described in the study by Rietveld and Ferreira [57]. Briefly, fluorescence spectral centers of mass at each concentration of urea were calculated as $\lambda_{[Urea]} = \sum\lambda I(\lambda)/\sum I(\lambda)$, where λ is the emission wavelength and $I(\lambda)$ is the fluorescent intensity at wavelength λ. The data were globally fitted to apparent two-state (for AMPPNP + methionine) or three-state (for no ligands, or in the presence of SAM) models of protein unfolding, as described in the study by Walters et al [58]. Briefly, the two-state model fit was performed using the following equation:

$$Y = ((\alpha_N + \beta_N \cdot [\text{urea}]) + (\alpha_U + \beta_U \cdot [\text{urea}])) \cdot \exp((-m \cdot [\text{urea}] - Cm))/RT)/(1 + \exp((-m \cdot [\text{urea}] Cm))/RT))$$

where Y is the apparent fraction of the unfolded protein, α_N and β_N are the native state signal at zero denaturant, and the slope of the native state baseline, α_U and β_U are the denatured state signal at 6 M urea, and the slope of the denatured state baseline, m is the transition slope (dependence of the free energy change on urea concentration, cal/mol/M), C_m is the concentration of urea at the midpoint transition, R is the ideal gas constant (1.987 cal/mol/K), and T is 298 K.

The three-state model fit was performed using the following equation:

$$Y = ((\alpha_N + \beta_N \cdot [\text{urea}]) + (\alpha_I + \alpha_U \cdot [\text{urea}]) \cdot (\exp((-m_{I-U} \cdot [\text{urea}] - C_{mI-U}))/RT)) \cdot \exp((-m_{N-I} \cdot [\text{urea}] - C_{mN-I}))/RT)/(1 + (1 + \exp((-m_{I-U} \cdot [\text{urea}] - C_{mI-U}))/RT) \cdot \exp((-m_{N-I} \cdot [\text{urea}] - C_{mN-I}))/RT))$$

where α_I accounts for the signal change at the pre-intermediate state, $m_{I\text{-}U}$ and $m_{N\text{-}I}$ are the slopes of transition between intermediate and denatured states and between native and intermediate states, and $C_{mI\text{-}U}$ and $C_{mN\text{-}I}$ are urea concentrations at midpoint transition between intermediate and denatured states and between native and intermediate states.

uMAT urea-induced dissociation kinetics

uMAT samples (4 μM) were prepared in Hepes pH 7.5, 10 mM KCl, 1 mM DTT, and 10 mM $MgCl_2$ without ligands or in the presence of either 0.4 mM ATP or 0.4 mM SAM. The uMAT dissociation kinetics was measured in SX20 stopped-flow (Applied Photosystems) by mixing the protein in 1:1 ratio with 6 M urea (3 M urea final concentration) prepared in the same buffer with a corresponding additive. The ensuing perturbation in tryptophan fluorescence (ex. 295 nm, em. 343 nm) was measured, and the obtained signal was fitted to a sum of two exponentials, as described [58]:

$$A(t) - A(\infty) = \sum A_i \cdot e(-k_i t)$$

where $A(t)$ is the amplitude at time t, $A(\infty)$ is the offset value, A_i is the change in signal for phase i, and k_i is the observed rate at phase i.

Bis-ANS and Sypro-orange fluorescence measurements

The ligands on the surface hydrophobicity and folding state of uMAT werr probed with 4′-Dianilino-1,1′-binaphthyl-5,5′-disulfonic acid (bis-ANS) (Sigma) and SYPRO-Orange (Sigma) fluorescence dyes. Two micromolar UuMAT in 20 mM MOPS-KOH pH 7.5, 10 mM KCl, 10 mM $MgCl_2$, and 1 mM DTT without ligands preincubated for 1 h at room temperature with either 5 mM ATP or 1 mM SAM were mixed with 10 μM bis-ANS or ×20 SYPRO-orange dyes. Fluorescence emission spectra were acquired with Cary Eclipse fluorescence spectrophotometer (Agilent) (bis-ANS: ex. 395 nm, em. 540–650 nm; SYPRO-orange: ex. 490 nm, em. 440–600 nm).

ThermoFluor assay

Two micromolar uMAT samples were prepared in 20 mM MOPS-KOH pH 7.5, 10 mM KCl, 10 mM $MgCl_2$, 1 mM DTT, and ×20 SYPRO-orange dye in the presence of one of the following: 1 mM ATP, 1 mM methionine, 1 mM AMPPNP, 1 mM AMPPNP + 1 mM methionine, 1 mM SAM, or no additives. All samples were preincubated for 30 min at room temperature and transferred to hardshell PCR plates (BioRad). Fluorescence spectra were obtained in CFX96 Touch™ Real-Time PCR machine (BioRad) using HEX channel (ex. 515–535 em. 560–580) with a 1°/min temperature ramp. The data were analyzed in accordance with the procedure described in the study by Lavinder et al. [36]. Two thermal transitions, 20–45 °C and 50–65 °C, corresponding to disintegration of the tetramer and unfolding of the monomer, respectively, were treated separately. The obtained spectra were normalized and globally fitted to

$$Y = (\alpha_N + \beta_N \cdot T) + \exp(m(T - T_m))/1 + \exp\exp(m(T - T_m)),$$

where Y is the normalized signal, α_N and β_N are the intercept and slope of baseline for the folded state, and m is exponential factor related to the slope of the transition at the apparent melting temperature, TM.

Thermal denaturation of uMAT

Two micromolar uMAT in 20 mM MOPS-KOH pH 7.5, 10 mM KCl, 10 mM $MgCl_2$, and 1 mM DTT were melted by 1 °C/min temperature ramp in a Cary Eclipse fluorescent spectrophotomer (Agilent), and the ensuing change in tryprophan fluorescence was followed (ex. 293 nm, em. 340 nm). The obtained signal was globally fitted to a two-state thermal unfolding model as described in the study by Jackson and Fersht [59]:

$$Y = ((\alpha_N + \beta_N \cdot T) + (\alpha_U + \beta_U \cdot T)) * \exp(-(\Delta H_m * (1 - T/T_m))/RT_0))/(1 + \exp(-(\Delta H_m * (1 - T/T_m))/RT_0))$$

where Y is the normalized signal, α_N and β_N are the intercept and slope of baseline for the folded state, α_U and β_U are the intercept and slope of baseline for the denatured state, ΔH_m is the enthalpy of denaturation at the transition midpoint, T_m is the midpoint of thermal denaturation, R is the ideal gas constant (1.987 cal/mol/K), and T_0 is 298 K. The change in the heat capacity was assumed to be zero.

Multiple sequence alignment

The multiple sequence alignments were produced using the T-COFFEE (Expresso) server [60] and visualized using BioEdit, version 7.0.5.

Structural alignment

Structural alignments were performed using PyMol. The alignment of uMAT and eMAT monomers covered 240 amino acids, out of 378 residues for uMAT monomer and 383 residues for eMAT monomer, and resulted in rmsd of 1.35 Å. For comparison, alignment of uMAT monomers from the same structure that covered 352 residues out of 378, resulted in rmsd of 0.73 Å. Structural alignment of uMAT dimer (PDB ID: 6RJS, 6RK5) and eMAT dimer (PDB ID: 1P7L) produced rmsd of 3.5 Å. The alignment covered 280 amino acids. For comparison, alignment of uMAT dimers from the same structure that covered 712 residues resulted in rmsd of 0.99 Å.

Interface analysis (PISA)

Interfaces of various MATs were characterized using protein interfaces, surfaces, and assembly (PISA) server [61]. The interface area is calculated by PISA as a difference in total accessible surface areas of isolated and interfacing structures divided by two. Change in the solvation free energy upon formation of the interface, $\mathbf{\Delta^i G}$ in kcal/mol, is calculated as a difference in total solvation energies of isolated and interfacing structures. Negative $\mathbf{\Delta^i G}$ corresponds to hydrophobic interfaces and does not include the effect of satisfied hydrogen bonds and salt bridges across the interface. PISA also predicts hydrogen-bonds and salt-bridges formation in the interface. The inter-dimeric interface of uMAT is comprised of four interacting surface patches. All the parameters pertaining to the inter-dimeric interface are presented as summation over four individual patches (Table 2). The individual parameters of each patch are summarized in Table S1.

MAT proteolysis assay

uMAT and eMAT proteins were incubated for 30 min at room temperature, in the presence or absence of SAM, before the addition of either trypsin or thermolysin. Final reaction conditions were as follows: 0.02 mg/ml trypsin/thermolysin, 20 mM Tris pH 8.0, 10 mM $CaCl_2$, 50 mM NaCl, 0.5 mg/ml MAT, 0.04 mM SAM (if added). The reaction was conducted at 37 °C and terminated at various time points by boiling the reaction aliquots in SDS loading buffer (40 mM Tris pH6.8, 1 mM SDS, 5% glycerol, and 50 mM DTT). Samples were run on 12.5% SDS-PAGE gel and stained using Coomassie Instant Blue (Expedeon).

Native-state MS

uMAT was diluted to 18 μM (monomer concentration) in 150 mM ammonium acetate at pH 8 (titrated with ammonia), and buffer exchanged into the same solution. SAM (20 mM, dissolved in 10 mM sulfuric acid) was diluted according to need in 150 mM ammonium acetate pH 8. For supplementation of the enzyme with SAM, 2 μl protein were mixed with 2 μl of different concentrations of SAM, to reach the required fold excess of MAT:SAM, and analyzed immediately.

Mass spectrometry (MS) measurements were done on a modified Q Exactive Plus EMR Orbitrap (Thermo) [62]. Samples were loaded into gold-coated nano-ESI capillaries, prepared in-house, as previously described [63] and sprayed into the mass spectrometer. Instrumental parameters included capillary voltage 1.7 kV, inlet capillary temperature of 180 °C, fore-vacuum pressure of 1.42 mbar. Trapping gas pressure was set to 2, corresponding to HV pressure of 5.55×10^{-5} mbar and UHV pressure of 1.48×10^{-10} mbar. Bent flatapole DC bias and gradient were set to 2.2 V and 25 V, respectively, and the HCD cell was operated at 40 V. Mass assignments were done using the SUMMIT 1.0 software [64]. Searches were restricted to complexes containing up to four MAT monomers, up to 12 SAM molecules and up to 8 potassium ions, with an error of up to 50 Da.

The stoichiometry of binding between uMAT and SAM was measured under constant uMAT concentration (9 μM monomer concentration) with SAM supplemented at increasing concentrations ranging from 0 to 2 mM. The binding of higher than 8 molecules of SAM to the tetramer is attributed to nonspecific binding, which is a drawback of the electrospray ionization method [38].

Accession numbers

Coordinates and structure factors have been deposited in the Protein Data Bank with accession numbers 6RJS, 6RK5, 6RKC, 6RK7, 6RKA.

Acknowledgements

The authors thank Amir Aharoni and Mickey Kosloff for insightful comments and help with preparation of the manuscript. This work was supported by Israel Science Foundation grant 1630/15 to S.B.

Author contributions

S.B. conceived the study. D.K. and F.G. performed the laboratory experiments. S.B and D.K analyzed the data. R.Z. solved the crystal structures. A.S. generated crystals, collected, and processed the crystallographic data. G.B.-N. performed the native-state MS measurements, and G.B.-N. and M.S. analyzed the MS data. S.B. wrote the manuscript.

Appendix A. Supplementary data

Supplementary data to this article can be found online at https://doi.org/10.1016/j.jmb.2019.09.003.

Received 26 June 2019;
Received in revised form 20 August 2019;
Accepted 4 September 2019
Available online 12 September 2019

Keywords:
X-ray crystallography;
Native-state MS;
Methionine S-adenosyltransferase;
Dihedral homotetramer;
Protein-protein interface evolution

References

[1] G.D. Markham, M.A. Pajares, Structure-function relationships in methionine adenosyltransferases, Cell. Mol. Life Sci. 66 (2009) 636–648.
[2] G.F. Sanchez-Perez, M. Gasset, J.J. Calvete, M.A. Pajares, Role of an intrasubunit disulfide in the association state of the cytosolic homo-oligomer methionine adenosyltransferase, J. Biol. Chem. 278 (2003) 7285–7293.
[3] J. Schlesier, J. Siegrist, S. Gerhardt, A. Erb, S. Blaesi, M. Richter, et al., Structural and functional characterisation of the methionine adenosyltransferase from Thermococcus kodakarensis, BMC Struct. Biol. 13 (2013) 22.
[4] F. Wang, S. Singh, J. Zhang, T.D. Huber, K.E. Helmich, M. Sunkara, et al., Understanding molecular recognition of promiscuity of thermophilic methionine adenosyltransferase sMAT from Sulfolobus solfataricus, FEBS J. 281 (2014) 4224–4239.
[5] M. Fontecave, M. Atta, E. Mulliez, S-adenosylmethionine, Nothing goes to waste, Trends Biochem. Sci. 29 (2004) 243–249.
[6] M.M. Sanchez del Pino, I. Perez-Mato, J.M. Sanz, J.M. Mato, F.J. Corrales, Folding of dimeric methionine adenosyltransferase III: identification of two folding intermediates, J. Biol. Chem. 277 (2002) 12061–12066.
[7] S.P. Zano, A.G. Pavlovsky, R.E. Viola, Structure of an unusual S-adenosylmethionine synthetase from Campylobacter jejuni, Acta. Crystallogr. D Biol. Crystallogr. 70 (2014) 442–450.
[8] E.D. Levy, E. Boeri Erba, C.V. Robinson, S.A. Teichmann, Assembly reflects evolution of protein complexes, Nature 453 (2008) 1262–1265.
[9] E.T. Powers, D.L. Powers, A perspective on mechanisms of protein tetramer formation, Biophys. J. 85 (2003) 3587–3599.
[10] G. Villar, A.W. Wilber, A.J. Williamson, P. Thiara, J.P. Doye, A.A. Louis, et al., Self-assembly and evolution of homomeric protein complexes, Phys. Rev. Lett. 102 (2009) 118106.
[11] J.A. Marsh, S.A. Teichmann, Structure, dynamics, assembly, and evolution of protein complexes, Annu. Rev. Biochem. 84 (2015) 551–575.
[12] M. Lynch, The evolution of multimeric protein assemblages, Mol. Biol. Evol. 29 (2012) 1353–1366.
[13] M. Lynch, Evolutionary diversification of the multimeric states of proteins, Proc. Natl. Acad. Sci. U. S. A. 110 (2013) E2821–E2828.
[14] S. Bershtein, W. Mu, E.I. Shakhnovich, Soluble oligomerization provides a beneficial fitness effect on destabilizing mutations, Proc. Natl. Acad. Sci. U. S. A. 109 (2012) 4857–4862.
[15] N.J. Fraser, J.W. Liu, P.D. Mabbitt, G.J. Correy, C.W. Coppin, M. Lethier, et al., Evolution of protein quaternary structure in response to selective pressure for increased thermostability, J. Mol. Biol. 428 (2016) 2359–2371.
[16] W.M. Jacobs, T.P. Knowles, D. Frenkel, Oligomers of heat-shock proteins: structures that don't imply function, PLoS Comput. Biol. 12 (2016) e1004756.
[17] K. Gunasekaran, B. Ma, R. Nussinov, Is allostery an intrinsic property of all dynamic proteins? Proteins 57 (2004) 433–443.

[18] V.J. Hilser, J.O. Wrabl, H.N. Motlagh, Structural and energetic basis of allostery, Annu. Rev. Biophys. 41 (2012) 585–609.
[19] J.W. Fairman, S.R. Wijerathna, M.F. Ahmad, H. Xu, R. Nakano, S. Jha, et al., Structural basis for allosteric regulation of human ribonucleotide reductase by nucleotide-induced oligomerization, Nat. Struct. Mol. Biol. 18 (2011) 316–322.
[20] K. Hashimoto, H. Nishi, S. Bryant, A.R. Panchenko, Caught in self-interaction: evolutionary and functional mechanisms of protein homooligomerization, Phys. Biol. 8 (2011) 035007.
[21] I.M. Nooren, J.M. Thornton, Structural characterisation and functional significance of transient protein-protein interactions, J. Mol. Biol. 325 (2003) 991–1018.
[22] L.T. Bergendahl, J.A. Marsh, Functional determinants of protein assembly into homomeric complexes, Sci. Rep. 7 (2017) 4932.
[23] B. Gonzalez, M.A. Pajares, J.A. Hermoso, L. Alvarez, F. Garrido, J.R. Sufrin, et al., The crystal structure of tetrameric methionine adenosyltransferase from rat liver reveals the methionine-binding site, J. Mol. Biol. 300 (2000) 363–375.
[24] F. Takusagawa, S. Kamitori, S. Misaki, G.D. Markham, Crystal structure of S-adenosylmethionine synthetase, J. Biol. Chem. 271 (1996) 136–147.
[25] S.H. Mudd, G.L. Cantoni, Activation of methionine for transmethylation. III. The methionine-activating enzyme of Bakers' yeast, J. Biol. Chem. 231 (1958) 481–492.
[26] J. Komoto, T. Yamada, Y. Takata, G.D. Markham, F. Takusagawa, Crystal structure of the S-adenosylmethionine synthetase ternary complex: a novel catalytic mechanism of S-adenosylmethionine synthesis from ATP and Met, Biochemistry 43 (2004) 1821–1831.
[27] G.D. Markham, E.W. Hafner, C.W. Tabor, H. Tabor, S-Adenosylmethionine synthetase from Escherichia coli, J. Biol. Chem. 255 (1980) 9082–9092.
[28] M.S. McQueney, K.S. Anderson, G.D. Markham, Energetics of S-adenosylmethionine synthetase catalysis, Biochemistry 39 (2000) 4443–4454.
[29] J.C. Taylor, G.D. Markham, Conformational dynamics of the active site loop of S-adenosylmethionine synthetase illuminated by site-directed spin labeling, Arch. Biochem. Biophys. 415 (2003) 164–171.
[30] J.C. Taylor, F. Takusagawa, G.D. Markham, The active site loop of S-adenosylmethionine synthetase modulates catalytic efficiency, Biochemistry 41 (2002) 9358–9369.
[31] P. Acharya, N.M. Rao, Stability studies on a lipase from Bacillus subtilis in guanidinium chloride, J. Protein Chem. 22 (2003) 51–60.
[32] M. Cardamone, N.K. Puri, Spectrofluorimetric assessment of the surface hydrophobicity of proteins, Biochem. J. 282 (Pt 2) (1992) 589–593.
[33] Y. Goto, A.L. Fink, Conformational states of beta-lactamase: molten-globule states at acidic and alkaline pH with high salt, Biochemistry 28 (1989) 945–952.
[34] A. Chari, D. Haselbach, J.M. Kirves, J. Ohmer, E. Paknia, N. Fischer, et al., ProteoPlex: stability optimization of macromolecular complexes by sparse-matrix screening of chemical space, Nat. Methods 12 (2015) 859–865.
[35] U.B. Ericsson, B.M. Hallberg, G.T. Detitta, N. Dekker, P. Nordlund, Thermofluor-based high-throughput stability optimization of proteins for structural studies, Anal. Biochem. 357 (2006) 289–298.
[36] J.J. Lavinder, S.B. Hari, B.J. Sullivan, T.J. Magliery, High-throughput thermal scanning: a general, rapid dye-binding thermal shift screen for protein engineering, J. Am. Chem. Soc. 131 (2009) 3794–3795.
[37] C. Park, S. Zhou, J. Gilmore, S. Marqusee, Energetics-based protein profiling on a proteomic scale: identification of proteins resistant to proteolysis, J. Mol. Biol. 368 (2007) 1426–1437.
[38] W. Wang, E.N. Kitova, J.S. Klassen, Influence of solution and gas phase processes on protein-carbohydrate binding affinities determined by nanoelectrospray Fourier transform ion cyclotron resonance mass spectrometry, Anal. Chem. 75 (2003) 4945–4955.
[39] J. Janin, S. Miller, C. Chothia, Surface, subunit interfaces and interior of oligomeric proteins, J. Mol. Biol. 204 (1988) 155–164.
[40] D.S. Goodsell, A.J. Olson, Structural symmetry and protein function, Annu. Rev. Biophys. Biomol. Struct. 29 (2000) 105–153.
[41] J.A. Marsh, H.A. Rees, S.E. Ahnert, S.A. Teichmann, Structural and evolutionary versatility in protein complexes with uneven stoichiometry, Nat. Commun. 6 (2015) 6394.
[42] E.D. Levy, J.B. Pereira-Leal, C. Chothia, S.A. Teichmann, 3D complex: a structural classification of protein complexes, PLoS Comput. Biol. 2 (2006) e155.
[43] E.D. Levy, S. Teichmann, Structural, evolutionary, and assembly principles of protein oligomerization, Prog. Mol. Biol. Transl. Sci. 117 (2013) 25–51.
[44] T. Maier, J. Marcos, J.A. Wodke, B. Paetzold, M. Liebeke, R. Gutierrez-Gallego, et al., Large-scale metabolome analysis and quantitative integration with genomics and proteomics data in Mycoplasma pneumoniae, Mol. Biosyst. 9 (2013) 1743–1755.
[45] S. Razin, D. Yogev, Y. Naot, Molecular biology and pathogenicity of mycoplasmas, Microbiol. Mol. Biol. Rev. 62 (1998) 1094–1156.
[46] P. Sirand-Pugnet, C. Citti, A. Barre, A. Blanchard, Evolution of mollicutes: down a bumpy road with twists and turns, Res. Microbiol. 158 (2007) 754–766.
[47] H. Weissbach, N. Brot, Regulation of methionine synthesis in Escherichia coli, Mol. Microbiol. 5 (1991) 1593–1597.
[48] P. Wong, W.A. Houry, Chaperone networks in bacteria: analysis of protein homeostasis in minimal cells, J. Struct. Biol. 146 (2004) 79–89.
[49] G.W. Clark, E.R. Tillier, Loss and gain of GroEL in the mollicutes, Biochem. Cell Biol. 88 (2010) 185–194.
[50] M.M. Gromiha, M.C. Pathak, K. Saraboji, E.A. Ortlund, E.A. Gaucher, Hydrophobic environment is a key factor for the stability of thermophilic proteins, Proteins 81 (2013) 715–721.
[51] D. Eisenberg, E. Schwarz, M. Komaromy, R. Wall, Analysis of membrane and surface protein sequences with the hydrophobic moment plot, J. Mol. Biol. 179 (1984) 125–142.
[52] W. Kabsch, Xds. Acta. Crystallogr. D Biol. Crystallogr. 66 (2010) 125–132.
[53] A.J. McCoy, R.W. Grosse-Kunstleve, P.D. Adams, M.D. Winn, L.C. Storoni, R.J. Read, Phaser crystallographic software, J. Appl. Crystallogr. 40 (2007) 658–674.
[54] M.D. Winn, C.C. Ballard, K.D. Cowtan, E.J. Dodson, P. Emsley, P.R. Evans, et al., Overview of the CCP4 suite and current developments, Acta. Crystallogr. D Biol. Crystallogr. 67 (2011) 235–242.

[55] P. Emsley, K. Cowtan, Coot: model-building tools for molecular graphics, Acta. Crystallogr. D Biol. Crystallogr. 60 (2004) 2126–2132.
[56] G.N. Murshudov, P. Skubak, A.A. Lebedev, N.S. Pannu, R.A. Steiner, R.A. Nicholls, et al., REFMAC5 for the refinement of macromolecular crystal structures, Acta. Crystallogr. D Biol. Crystallogr. 67 (2011) 355–367.
[57] A.W. Rietveld, S.T. Ferreira, Kinetics and energetics of subunit dissociation/unfolding of TIM: the importance of oligomerization for conformational persistence and chemical stability of proteins, Biochemistry 37 (1998) 933–937.
[58] J. Walters, S.L. Milam, A.C. Clark, Practical approaches to protein folding and assembly: spectroscopic strategies in thermodynamics and kinetics, Methods Enzymol. 455 (2009) 1–39.
[59] S.E. Jackson, A.R. Fersht, Folding of chymotrypsin inhibitor 2. 1. Evidence for a two-state transition, Biochemistry 30 (1991) 10428–10435.
[60] C. Notredame, D.G. Higgins, J. Heringa, T-Coffee, A novel method for fast and accurate multiple sequence alignment, J. Mol. Biol. 302 (2000) 205–217.
[61] E. Krissinel, K. Henrick, Inference of macromolecular assemblies from crystalline state, J. Mol. Biol. 372 (2007) 774–797.
[62] G. Ben-Nissan, M.E. Belov, D. Morgenstern, Y. Levin, O. Dym, G. Arkind, et al., Triple-stage mass spectrometry unravels the heterogeneity of an endogenous protein complex, Anal. Chem. 89 (2017) 4708–4715.
[63] N. Kirshenbaum, I. Michaelevski, M. Sharon, Analyzing large protein complexes by structural mass spectrometry, J. Vis. Exp. (40) (2010) e1954.
[64] T. Taverner, H. Hernandez, M. Sharon, B.T. Ruotolo, D. Matak-Vinkovic, D. Devos, et al., Subunit architecture of intact protein complexes from mass spectrometry and homology modeling, Acc. Chem. Res. 41 (2008) 617–627.